JOURNAL OF COLLOID AND INTERFACE SCIENCE **185,** 217–227 (1997)
ARTICLE NO. CS964593

Scanning Transmission X-Ray Microscopy: A New Method for the Investigation of Aggregation in Silica

THEO P. M. BEELEN,*[,1] WEIDONG SHI,† GRAEME R. MORRISON,† HAROLD F. VAN GARDEREN,* MIKE T. BROWNE,† RUTGER A. VAN SANTEN,* AND EMMANUEL PANTOS‡

**Schuit Institute of Catalysis, Eindhoven University of Technology, P.O. Box 513, 5600 MB Eindhoven, The Netherlands; †Department of Physics, King's College London, Strand, London WC2R 2LS, United Kingdom; and ‡Daresbury Laboratory, Warrington WA4 4AD, United Kingdom*

Received April 12, 1996; accepted September 9, 1996

During the preparation of silica by acidification of water glass, primary silica particles form extended and ramified aggregates. The growing aggregates form a gel, a tenuous network of interconnected aggregates. After aging and drying of the wet gel, porous silica is obtained. To study the extremely vulnerable aggregates only noninvasive methods are allowed. Moreover, because of the colloidal scale many methods based on (atomic or molecular scale) spectroscopy are not informative. Scanning transmission x-ray microscopy (STXM), using high-brilliance synchrotron radiation at 3.25 nm (380 eV) and 2.60 nm (480 eV) as an X-ray source, provides a new technique to obtain direct images of wet or solved aggregates at a 50–5000 nm scale. The 50 nm resolution is sufficient to provide excellent images of fractal structures. In this paper the principles of STXM are discussed in relation to investigations of wet gel systems like silica gel. © 1997 Academic Press

Key Words: **STXM; X-ray microscopy; aggregates; fractal; silica; colloids.**

INTRODUCTION

For the great manifold of practical applications (catalyst support, filling agent, abrasive, isolating materials, ceramics, filter agents) many different types of silica are required, with surface reactivity, porosity, and pore size distribution as the most important parameters. Tailor-made preparations are necessary to satisfy the demands of the different products.

Commercially, bulk quantities of silica are prepared by controlled acidification of water glass (alkali solution of silica). Polymerization (polycondensation) reactions occur between dissolved oligomeric silica species, resulting in (sub)-colloidal particles. The rate of formation and the size of these particles are strongly pH-dependent (1).

At low pH, or after screening by electrolytes of negative surface charge, silica particles may form interparticle bonds due to condensation reactions between -SiOH and -SiO^- groups on different primary particles. Because the distribution of reactive groups on the surface of the particles is stochastic, directions of particle–particle bonds are rather arbitrary and therefore particle–particle interactions result in tenuous aggregates with an amorphous structure. Interactions are not restricted to particle–particle or particle–aggregate bonds, and interactions between aggregates or clusters of particles are also possible, leading to highly ramified and extended aggregates.

Polymerization or particle formation and aggregation, however, are not strictly sequential processes: both are based on the same (condensation) reaction and therefore are to be considered parallel processes. Moreover, because OH^- is both a reagent and a catalyst for the condensation/hydrolysis reaction, reaction rates at low pH are much lower than at high pH and are comparable to diffusion rates of small particles. Therefore, before elementary particles have grown to maximum size, aggregates may be formed by either reaction-limited or diffusion-limited cluster–cluster aggregation, depending on the ratio between reaction and diffusion rates. At high pH, condensation rates are much higher and in combination with increasing SiO^-/SiOH ratios, much bigger elementary particles and relatively small aggregates are formed.

If the acidified water glass solution contains sufficient silica, the growing aggregates impinge on one another, forming a percolating system: the gel. Especially at low pH (small particles) the gel can be visualized as a tenuous network of interconnected aggregates with the silica density mainly concentrated in the centre of the aggregates. The branches of the aggregates are relatively thin threads composed of chains of silica particles (2). Voids between the aggregates or within the branches of the aggregates are still filled with a solution containing silica as monomers, oligomers, primary particles, and small aggregates. After the gelation point this silica is added gradually to the thin threads, reinforcing the weak gelatinous system.

After acidification, aggregation, and gelation, silica gel is still far from thermodynamic equilibrium. By a dynamic balance of condensation and hydrolysis, a continuous process of dissolving and recondensation of monomers or oligo-

[1] To whom correspondence should be addressed.

0021-9797/97 $25.00

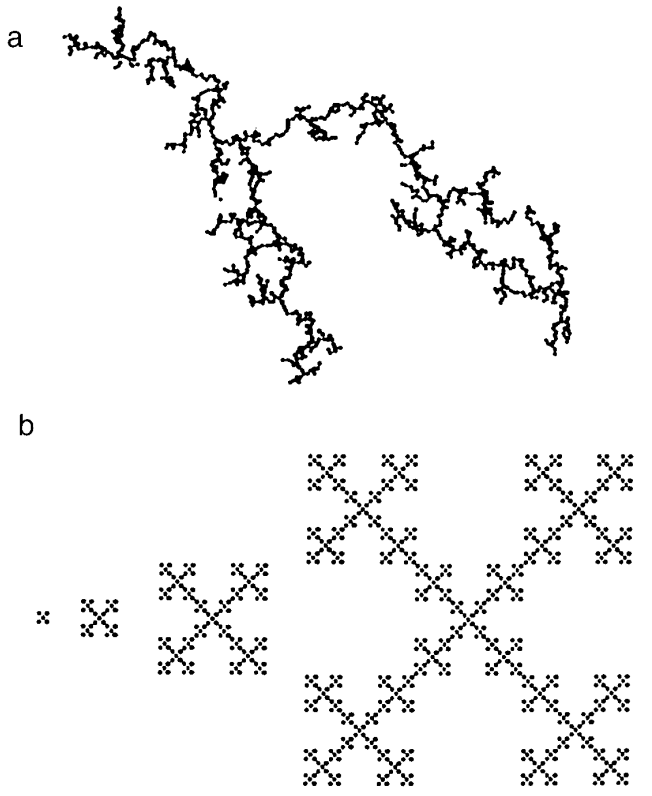

FIG. 1. (a) Fractal aggregate, constructed by computer-simulated diffusion-limited aggregation. Fractal dimension $D = 1.44$. (b) Deterministic Vicsek fractal constructed of 1, 5, 25, and 125 basic units respectively. Fractal dimension $D = 1.465$.

mers of silica will change the form of the network. Due to the difference in surface energy, silica at highly curved surfaces (convex surfaces) will dissolve relatively easy and recondense preferentially in the ''necks'' between particles or in the crevices in the centre of the aggregates (concave surfaces). This effect (Ostwald ripening) decreases the number of small particles and smoothes the chains or surfaces of the gel network and is the main contribution to the aging process (1). During aging the gel network is reinforced considerably and will be stronger in withstanding the capillary forces during drying, resulting in a porous structure of dried silica. Without sufficient aging the weak gel structure will collapse during drying and only a microporous silica would be produced (3–5). Therefore, to obtain porous silica, reinforcement of the weak and tenuous structures by aging processes is necessary (1, 2).

To characterize stochastic processes such as aggregation and gelation and subsequent transformations during aging, fractal concepts are almost indispensible. Introduced to the scientific community rather recently [Mandelbrot's ''The Fractal Geometry of Nature'' was published in 1977 (6)], many phenomena in physics, chemistry, and biology can be described using fractal principles, including aggregation (7, 8). To explain basic principles of fractal analysis we will use two-dimensional models of aggregates depicted in Fig. 1.

In Fig. 1a an aggregate is shown with a mass density gradient: mass distribution in the center is distinctly different (higher average density) compared with the mass density in the periphery. As will be shown in the next paragraphs this mass distribution and its gradient is determined by the physics of the aggregation process and therefore related to the process parameters. Moreover, the aggregate is (in a statistical sense) self-similar: the same gradient in density distribution is observed on different length scales, resulting in a characteristic quantity or variable for the density gradient: the fractal dimension. This concept is easier to understand with the growth of an ''artificial aggregate'' in Fig. 1b, known as Vicsek's 2D deterministic fractal (8, 9). As shown, this can be constructed by adding the figure repeatedly to its corner points, each iteration resulting in a threefold increase in size R. The ''mass'' M (= number of points), however, is increasing only fivefold at each step (instead of ninefold according to Euclidean geometry), resulting in the relation $M \approx R^D$ with $D = \log 5/\log 3 = 1.465$, as can be shown easily (8). Contrary to the mass–size relations in (two-dimensional) Euclidean geometry with $M \approx R^2$, in Vicsek's fractal one is dealing with a non-integer (''fractal'') dimension ($D = 1.465$) for this relation. The mass distribution of fractal systems shows a typical behavior: mass density is not a constant but depends on R or any other representative length scale. So, unlike in Euclidean systems, one can observe a non-zero mass density gradient, described by the fractal dimension D.

In non-deterministic fractal systems like the aggregate in Fig. 1a, the mass density also decreases with increasing R, but now D [determined with statistical methods (7, 9)] is 1.44 [the corresponding aggregate in three-dimensional space has $D = 1.81$ (9)]. Although shape and morphology are quite

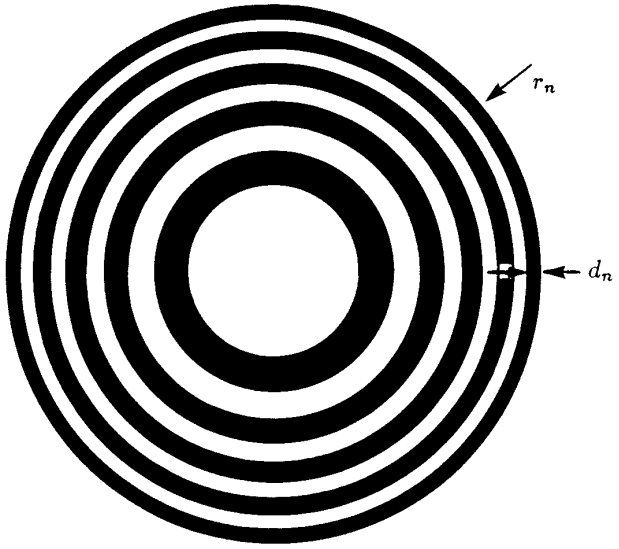

FIG. 2. A schematic diagram of a Fresnel zone plate.

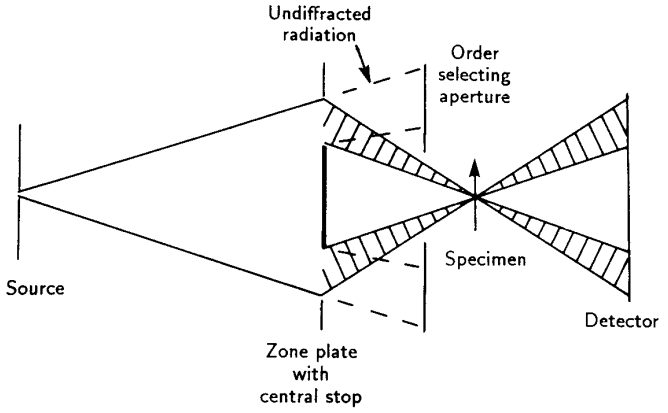

FIG. 3. Optical configuration for a STXM.

different, the fractal dimension D and therefore the decrease in mass density are almost the same in Fig. 1a and 1b. With the concept of fractal dimension, differences or similarities in mass density distributions between aggregates may be quantified, such as changes due to growth and aging. Therefore the fractal dimension can be considered to be an important parameter to describe aggregation, gelation, and aging phenomena in silicas, comparable to other system parameters such as density or porosity.

During aging silica is redistributed in the gel. Although this redistribution is based only on hydrolysis/recondensation reactions of silica monomers, oligomers, or particles, many different transformations and structures may be formed, depending on the process parameters (temperature, concentration, pH, catalysts). During aging the fractal dimensions can both increase and decrease, depending also on the size of aging structures (10, 11). This variety in aging processes makes an important contribution to the wide range of porous silica structures available.

The investigation of aging mechanisms is quite challenging. Although understanding aging reactions is necessary to prepare tailor-made porous silicas on a scientific basis, the choice of proper methods and techniques to study wet gels is difficult. The vulnerability of the fragile systems requires that only a very few non-invasive methods may be used, for example ^{29}Si-NMR (12, 13) and especially small angle scattering with X rays (SAXS) or neutrons (SANS) (5, 11, 14, 15). The extended length scale of aggregation, gelation, and aging (more than four decades: from sub-nanometer to a few microns), however, calls for the combination of NMR, SAXS, or SANS with techniques able to investigate aggregates, wet gels, or aging processes in silica in the range between 100 nm and 20 microns. In this paper we will show that STXM is an appropriate method to study wet silicas at this length scale.

SCANNING TRANSMISSION X-RAY MICROSCOPY (STXM)

Because X rays cannot be focused by lenses of glass (visible light microscopy) or magnets (electron microscopy), other reflective or diffractive optical elements have to be found. To date, the most successful high-resolution X-ray microscopes (16–18) use Fresnel zone plates as diffractive focusing elements. A zone plate is a form of circular diffraction grating that has a radially increasing line density, as is shown in Fig. 2. These gratings are used in transmission and generally consist of alternate transmitting and absorbing zones. A zone plate consisting of n such zones may be shown by a simple analysis to produce an infinite number of diffraction orders, with the property that parallel illumination incident on the zone plate is brought to focus at a distance f_m from the zone plate, with

$$f_m = r_n^2/mn\lambda$$

where m is the diffraction order, r_n is the radius of the nth zone, and λ is the wavelength of the incident radiation. When monochromatic radiation is incident on a zone plate with a large number of zones, the focal spot is found to resemble very closely an Airy disc whose diameter (out to the first intensity zero) is given by $1.22d_n/m$, where d_n is the width of the nth zone, so the secret of achieving high-resolution images is to be able to fabricate zone plates with very fine outermost zones. At present, the best available zone plates have outermost zones that are only a few tens of nanometers wide, and to achieve the highest possible focusing efficiency the zone plates are operated using the first-order diffraction focus. For the experiments discussed in this paper the outermost zone was either 37 or 50 nm and the zone plate was fabricated by P. S. Charalambous at King's College (London).

Because of the need to have a high X-ray flux on a very small area of the specimen, and because the combination of monochromator and zone plate reduces the intensity of the focused X-ray beam considerably, very intense (high-bril-

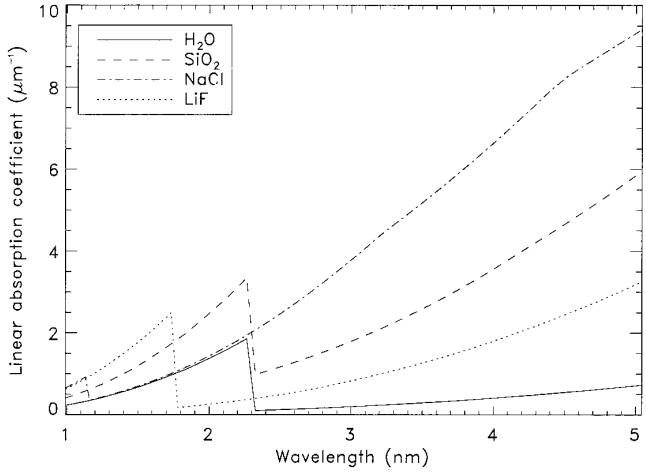

FIG. 4. Linear absorption coefficients as a function of wavelength in the region for silica and water.

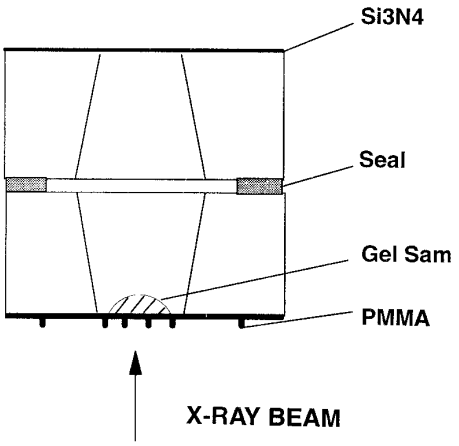

FIG. 5. STXM-cell, size 6 mm × 6 mm.

liance) X-ray sources are necessary. With the advent of synchrotron radiation sources (and the application of microcircuit fabrication techniques to the production of zone plates) instrumental development has recently been quite rapid. There are now active programs to develop X-ray microscopy at a number of laboratories throughout the world, and working instruments have already been installed on the synchrotron radiation sources at BESSY (Berlin, FRG), the NSLS (Brookhaven, USA), the SRS (Daresbury, UK), the Photon Factory (Tsukuba, Japan), and ELETTRA (Trieste, Italy).

In Fig. 3 the essential elements of the optics of an STXM are shown (17). The focusing element (zone plate) forms a demagnified image of the source on the specimen plane, usually the exit slit of some form of soft X-ray monochromator. To maximize the available intensity the brilliance (intensity per square mm per unit solid angle per unit bandwidth) of the X-ray source must be as large as possible. For this reason an insertion device such as an undulator is often used to enhance the source brilliance. The STXM at Daresbury Laboratory is installed on undulator beam line 5U2 (16).

Figure 3 also shows that undiffracted (unfocused) radiation is prevented from reaching the specimen by a central stop on the zone plate. Higher diffraction orders as well as undiffracted radiation are removed by the order-selecting aperture.

Having produced a focused X-ray probe, an image is formed by mechanically scanning the specimen in a raster perpendicular to the beam direction and measuring the transmitted flux as a function of specimen position. In order that the image resolution is determined by the probe-forming optics and not by the coarseness of the sampling grid imposed on the scanning raster, it is important that the specimen can be moved in increments smaller than the probe size. This can be achieved (16, 17) by means of a specimen stage driven by piezo-electric transducers, possibly with some form of feedback mechanism being used to reduce the nonlinearities in the response of these devices. As the data for each picture point are acquired sequentially, the image acquisition time is proportional to the number of pixels in the image. It is therefore essential to have a high intensity in

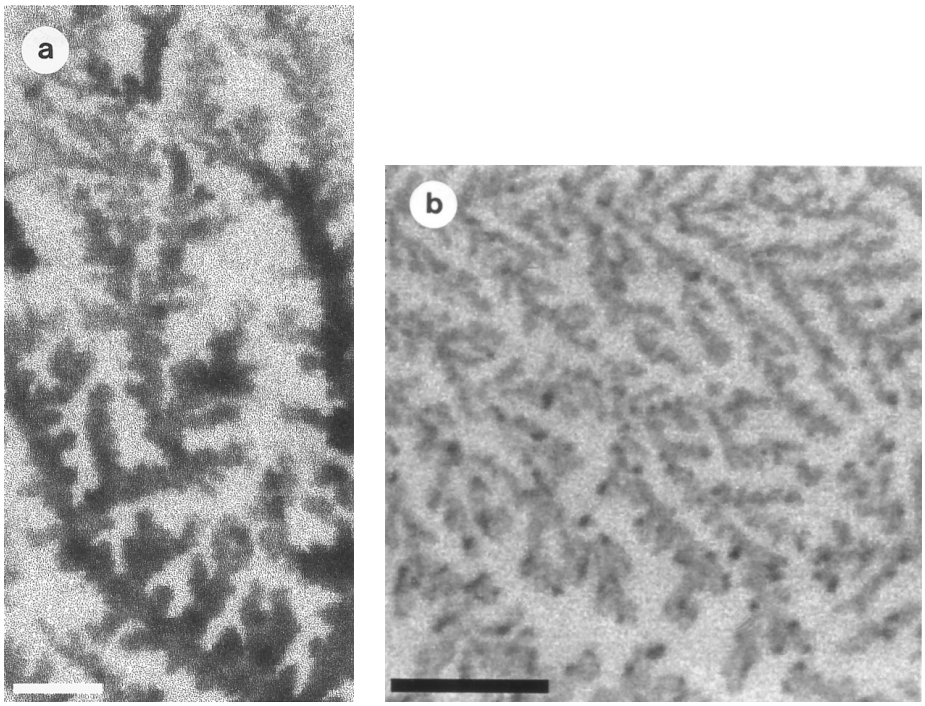

FIG. 6. Examples of fractal aggregates, observed by STXM after evaporation of water. (a) pH = 4, 4 wt % SiO_2, K water glass. Bar = 4 μm. (b) pH = 3, 0.4 wt % SiO_2, Na water glass. Bar = 5 μm.

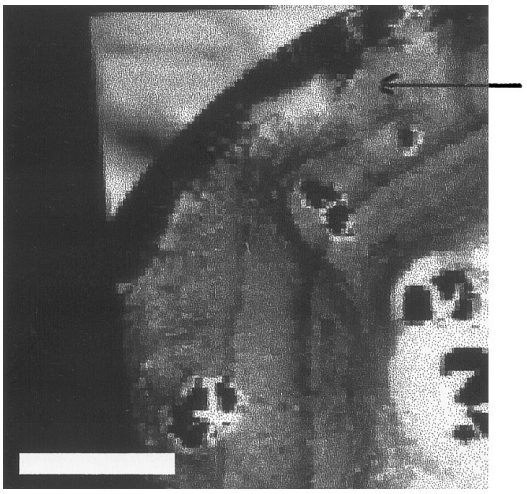

FIG. 7. Overview of solids deposited onto the window after drying of the silica solution. Bar = 200 μm.

the focused probe, so that the dwell time per pixel needed to achieve a reasonable signal to noise ratio in the image is not unacceptably long. Using an efficient electronic detector such as a gas flow proportional counter, the serial image data is collected in digital form and is displayed on a video framestore, so it is immediately available for inspection or processing without further irradiation of the specimen.

Many general aspects of X-ray microscopy and especially a discussion of physical backgrounds can be found in a recent lead article in *Acta Crystallographica* by Sayre and Chapman (20).

One of the main reasons for developing a microscope to operate at soft X-ray wavelengths was to take advantage of the so-called ''water window'' lying between the oxygen and carbon K absorption edges. X rays in this region of the spectrum are absorbed strongly by organic matter but much less so by water. The same principle can be applied for silica, and in Fig. 4 is shown a graph of the X-ray absorption coefficient for silica and water for wavelengths in the soft X-ray region. Images discussed in this paper have been monitored using synchrotron radiation at 3.25 nm (380 eV) and 2.6 nm (480 eV).

With the STXM, information can be obtained about features with sizes between 50 nm and 100 micron (16–19). These length scales are representative for aggregation and gelation in many types of silica gels (21–24) as well as suspensions of hematites (25) and clays (26). Because STXM exploits the so-called ''water window'' of X-ray wavelengths, it is very suitable to investigate sols, growing aggregates, and wet (aging) gels without disturbing the fragile gels or aggregate structures. In comparison to microscopy with visible light, optically transparent samples are *not* required and a higher resolution can be obtained. Although the wavelength of electrons in electron microscopy is still smaller, resulting in better resolution, the interaction cross section for X rays is much smaller than for electron scattering so that samples with thickness up to 10 microns may be investigated with STXM, and these specimens need not to be maintained under high-vacuum conditions while they are being examined.

The present technical improvements to the methods of microfabrication that now permit zone plates as diffractive focusing elements to be produced and the development of high-brilliance synchrotron radiation sources have led to the recent resurgence of interest in X-ray microscopy at soft X-ray wavelengths. The advent of ''third generation'' synchrotrons (ESRF, France) with a source brilliance that is up to 3 orders of magnitude higher should allow further rapid development of X-ray imaging techniques.

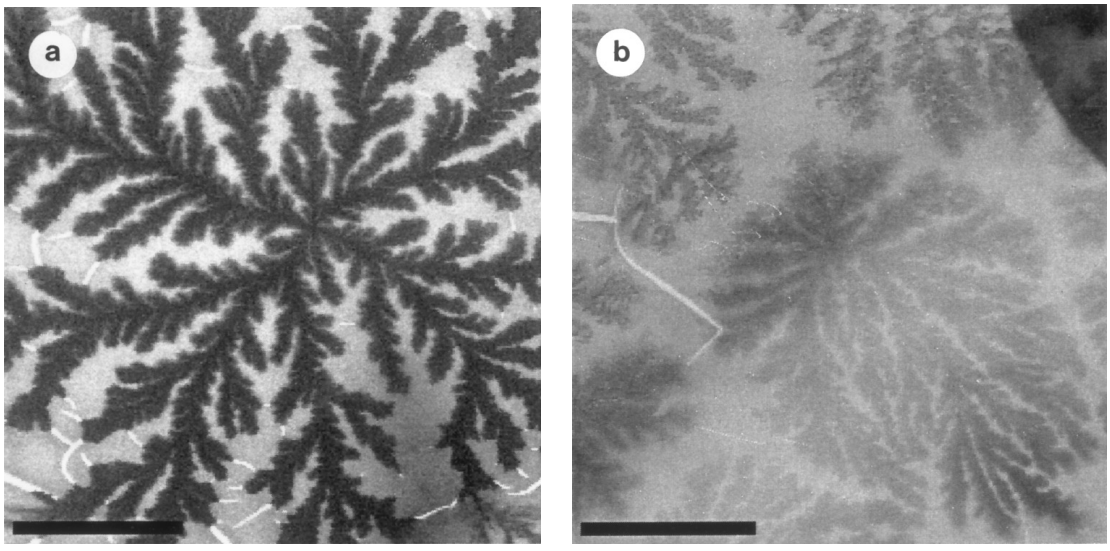

FIG. 8. Examples of fractals not influenced (a) and influenced (b) by the direction of drying. Bars are 50 μm.

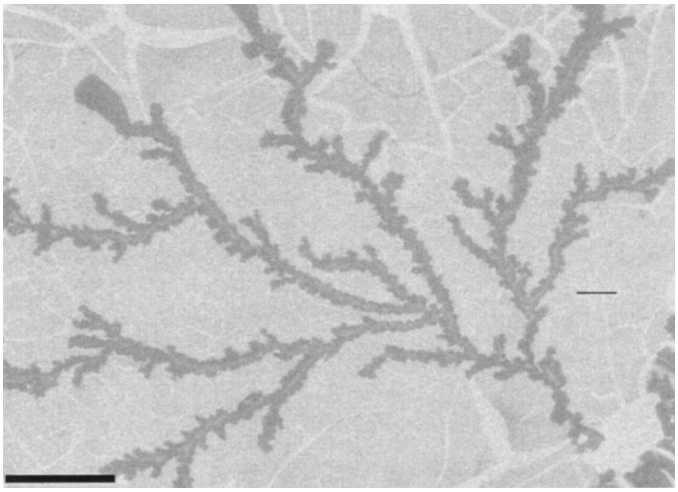

FIG. 9. Salt-saturated fractals. Bar = 30 μm.

EXPERIMENTAL

Some samples of water glass solutions were prepared by dissolution of amorphous silica (Aerosil 200 and 380, a gift from Degussa AG) in sodium hydroxide (Merck p.a.) using Teflon or polyethylene beakers. Others were prepared by dissolution of fumed silica powder (CAB-O-Sil, M-5) in NaOH under vigorous stirring and at solution temperatures up to 70°C in order to accelerate the dissolution of the silica powder. In a typical experiment the overall molar composition was chosen to be SiO_2:NaOH:H_2O = 3:2:125. Silica gels were prepared by acidification of the alkaline silica solutions. The water glass solution was dosed drop by drop with a Pasteur pipette to a solution of 1.0 *M* HCl while stirring vigorously until the desired pH was reached. During gelation the stirring was stopped. Gelation time was the period of time elapsed between the end of acidification and the moment when no meniscus deformation could be observed on twisting the beaker. However, because it was impossible to put a gel into the STXM-cell without destroying the extremely vulnerable windows, only solutions before the gel point were transferred in the cell using a syringe. Diluted systems (SiO_2 < 1 wt %) did not contain enough silica to create a continuous network and therefore could not gelate. To avoid evaporation, aging of acidified silica solutions was performed in closed containers. When the catalytic influence of fluorine was investigated, appropriate quantities of NaF were added to the HCl solution before acidification.

The STXM cell (Fig. 5) uses two 100 nm thick Si_3N_4 membranes as X-ray windows, and stresses associated with the transition of the fluid to a gel were often sufficient to shatter these windows. The use of small window apertures (1.6 × 1.6 mm^2) and the reinforcement of the membranes with bars of 2 micron thick PMMA polymer decreased the number of windows broken during imaging. To prevent fast drying of fluids, the two window frames are sealed together with glue. The rate of evaporation could be varied by using only a partial seal between the silicon frames.

RESULTS AND DISCUSSION

The first STXM images were made of quickly drying systems in an open cell. A solution of silica prepared by acidification of water glass to pH 4 was diluted and aged at room temperature for a week. Because the silica concentration was approximately equal to 0.1 wt % SiO_2, no gelation occurred. After putting a very small droplet of the aged silica solution on the Si_3N_4 window and then mildly heating the sample using the focused illumination of a visible light microscope, the water evaporates rather quickly and micron-sized aggregates can be observed (Fig. 6). Although the presence of (adsorbed) water could be demonstrated at the branches of this structure using FT-IR spectroscopy, we consider these aggregates as ''dry'' systems.

For the aggregates the relation $M = cL^D$ holds with $D \approx 1.55 - 1.7$, so the aggregates can be considered to be (possibly two-dimensional) fractals with (mass)fractal dimension *D* (7), similar to the fractal in Fig. 1a.

Concerning the origin of these aggregates there are two possibilities. The simpler explanation is that these micron-sized fractals were already present in the solution before drying, the aggregation process continuing from the nano scale all the way to the micron scale. The fractal range would be more than four decades (!), since SAXS measurements show that fractal aggregates can be observed all over the available SAXS range (1–70 nm) in this type of solution (3, 11, 21). The extension from the nano to the micro scale is confirmed by USAXS, showing a straight line in a log(*I*)–log(*Q*) plot in the range 50–1000 nm (21). However, the fractal dimension of aggregates observed by SAXS or USAXS is higher (D = 1.9), but because especially the USAXS range was very sensitive to background corrections (21), a small decrease in fractal dimension at larger length scales might be possible. This type of multifractality has also been observed in aging systems at smaller length scales both experimentally (10) and using computer simulations (11). Comparing the two-dimensional *D* from STXM with the three-dimensional *D* of SAXS/USAXS may seem unrealistic, but according to Mandelbrot projecting three-dimensional fractals with $D < 2$ on a two-dimensional plane will preserve this fractal dimension *D*. However, because this is only true for infinite fractals, to interpret fractal images made by electron microscopy Jullien and co-workers (27) analyzed the finite aggregate size effects on the preservation of *D* during projection, resulting in corrections in the order of 0.1–0.2. Therefore the very open fractal structure with D = 1.55–1.7 in three dimensions is represented by the same fractal dimension in a plane projection, although in this case the structure will appear somewhat denser.

Nevertheless, a decrease (or no change) in fractal dimen-

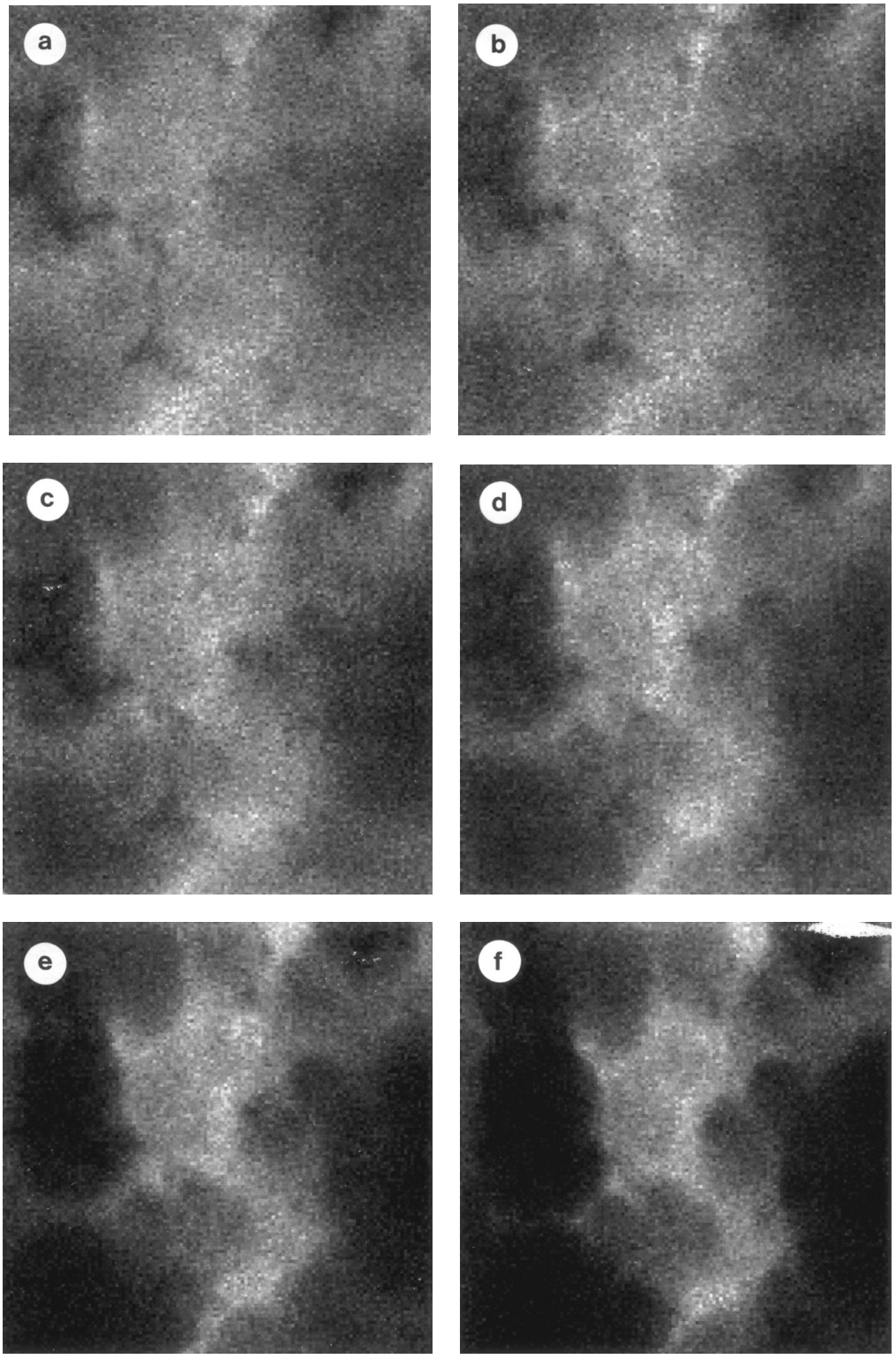

FIG. 10. Time sequence of growth process in silica (SiO_2/NaOH = 1/1, pH 7, 0.4 wt % SiO_2). Bar = 0.7 μm. (a) 31 min, (b) 43 min, (c) 61 min, (d) 84 min, (e) 106 min, (f) 126 min, (g) 149 min, (h) 193 min, and (i) 304 min.

sion during drying is not expected, because silica aggregates or gels will collapse during drying due to capillary forces when water is removed. This results in considerable shrinking and only in well-aged systems may pores be preserved, when ''protected'' by reinforced branches formed during aging, preferably in or near the center of aggregates (15). It

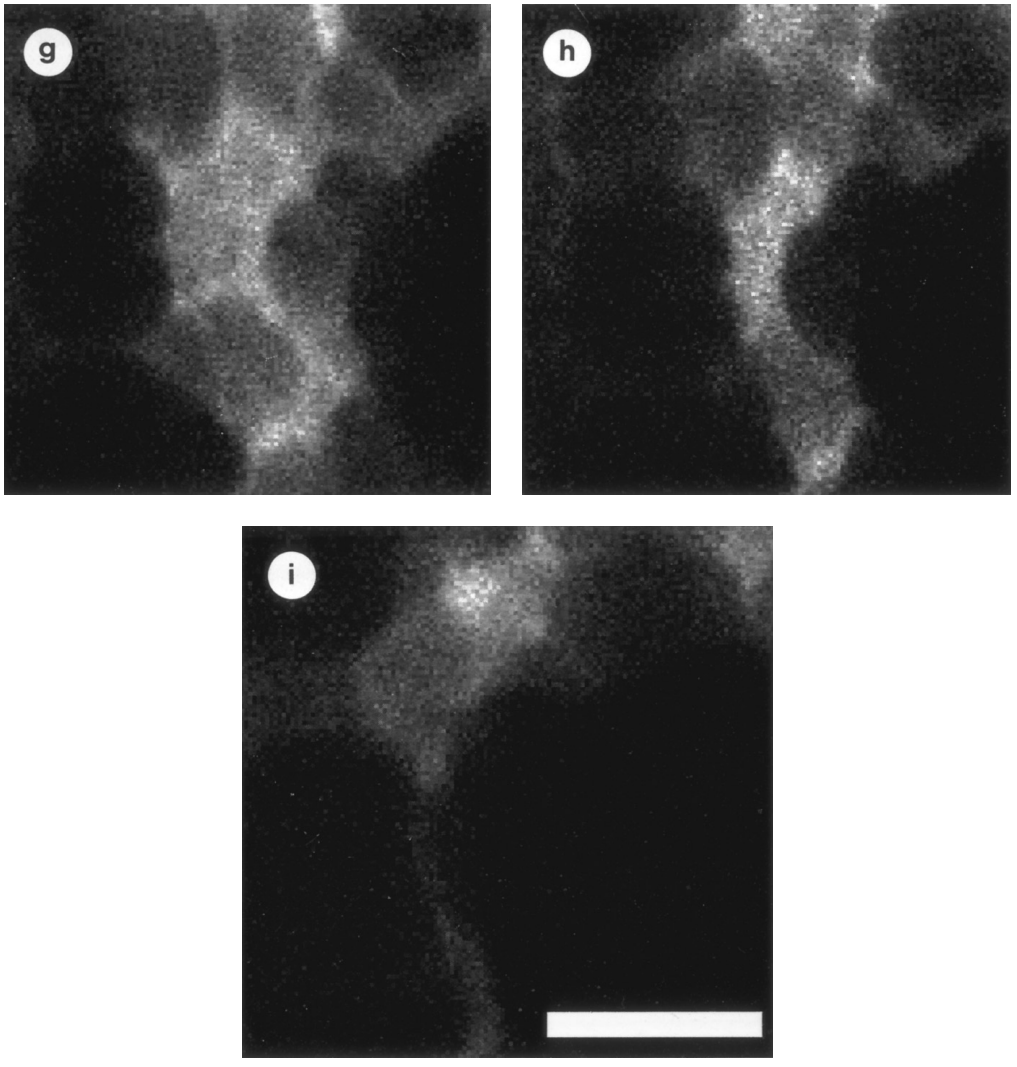

FIG. 10—*Continued*

is possible that at the micron scale the effect of a structural collapse at the nanometer scale cannot be observed. The strong micron-scaled backbone is preserved with a relatively open structure, but measurements on small local scale would show a higher fractal dimension. This process might be very similar to ''large-scale aging'' observed by SAXS experimentally (11) or using simulations (10), with mass transport by collapse instead of aging.

Despite repeated attempts, we were not able to observe the same kind of fractal structure in solution. One possible explanation is that at room temperature diffusion-driven movements of the branches of the aggregates were too large during the time scale of minutes needed for image acquisition. Even in the confined micron-sized space of the small droplets the aggregates have enough freedom to move and will not stick to the window.

Finally, we have to realize that one has to be optimistic to expect the same fractal dimension all over the four decades of the observed nanometer–micrometer range. Several important physical processes change considerably over this large range, for example diffusion, and also considerable differences in bonding have to be expected. Especially this last effect may be important: without doubt the colloidal forces in the formation of aggregates are scale-dependent and may even (partly) bridge the crossover between diffusion- and reaction-limited aggregation.

There is another possibility to consider when trying to explain the formation of the micron-scale aggregates. As the size of the aggregates is much smaller (order of magnitude 100–200 nm), during the contraction of the droplet (in the diluted system) freely moving aggregates will impinge on each other and can form aggregates at micron scale. The aggregates at nanometer scale can be considered to be the primary particles for aggregation at micrometer scale. Because the aggregates at nanometer scale are aged, they are reinforced sufficiently to behave like spherical particles.

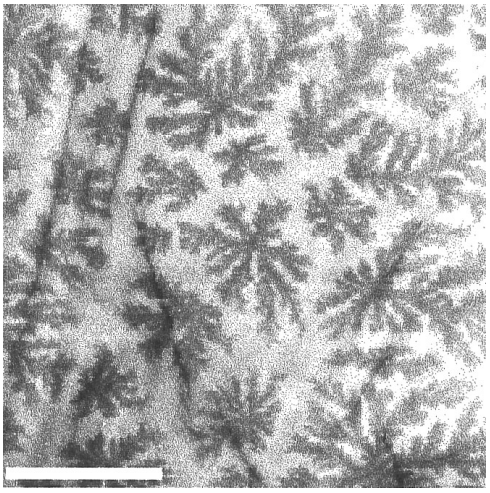

FIG. 11. Aggregates formed during the preparation of silica at pH 7. See Fig. 6b for preparation conditions. Bar = 50 μm.

Analogous ''second generation'' aggregates have been observed during the preparation of zeolites (28). This model is supported by two other observations. First, as shown in Fig. 7, aggregates are always observed near the periphery of the drying droplet (the arrow in this figure indicates the position of the fractal shown in Fig. 6a). It is possible that the aggregate is formed by (forced) diffusion-limited cluster–cluster aggregation in the quickly decreasing confined space of the retreating droplet during evaporation. In the center, where the majority of the mass is deposited, there is a big heap of aggregates and salt that is not transparent to X rays. Second, sometimes fractals indicate very clearly the direction of drying. For example, in Fig. 8 two fractal systems are shown from two different images of the same silica sample. In Fig. 8a no preferred direction can be observed, but in Fig. 8b we are sure that the supply of particles coming from the bottom right was much bigger than from other directions due to the withdrawal of water toward the upper-left. Unlike the nano-scaled SAXS experiments, it proved to be rather difficult to reproduce the fractal patterns produced by drying of aged solutions of silicas in open STXM cells because of the variation in drying conditions controlling the ballistic or enforced diffusion-limited aggregation process in the shrinking droplet.

In other phase-separating systems similar types of fractals have also been observed. For example, Deutscher and Lereah (29, 30) showed that during annealing of amorphous Al-Ge alloys phase separation resulted in the formation of fractal germanium aggregates very similar to our aggregates. The fractal properties were dependent on a complicated competition between atomic diffusion of Ge in Al, the diffusion-controlled growth of Ge and nucleation of new Ge crystallites at the Al–Ge interface. Also Duan Jian-zhong and coworkers (31, 32) prepared Pd–Si alloy films and observed the formation of Si fractals during annealing between 200 and 500°C. Although materials and reaction conditions were very different, both crystalline Si and our SiO_2 are in fact ''negative'' fractals (31), formed by withdrawal of Pd (formation of Pd_2Si by the reaction 2 $PdSi \rightarrow Pd_2Si + Pd$) and water respectively from the reaction mixture. In both cases the number of collisions by diffusing particles is enhanced considerably resulting in the formation of fractal aggregates. If reaction conditions are changed, for example by careful drying of a solution with a high (30%) concentration of silica only non-fractal cracks in the gel can be observed (33) although the regular pattern of these cracks is related to the gel structure (33). The relative rate of withdrawal of water is also very important, because if systems are growing by the very slow creation of a supersaturating solution, only surface fractals may be observed as is shown by Honjo and Ohta in their elegant experiments concerning the formation of crystals from a NH_4Cl solution (34).

It seems probable that the results of STXM (formation of micron-scaled aggregates during drying) and SAXS/USAXS (formation of micron- and nano-scaled aggregates in solution) are consistent, since the combined experimental evidence from both methods gives strong indications that the aggregates observed with USAXS might be the ''nuclei'' of the aggregates observed with STXM. Our main argument is that undisturbed diffusion on micron scale is an extremely slow process, especially compared to diffusion on the nanometer scale. Therefore we can observe the formation of fractals up to 50 nm within a few minutes (4 wt % SiO_2) (3), but the growth will continue during a very long time, even after gelation (approximately 1 h after the start of the experiment). This means that after the formation of the first big aggregates, many small aggregates or even primary particles are still diffusing freely and the number of collisions will decrease strongly when these aggregates and particles combine with bigger systems resulting in a more and more particle-depleted solution. This model is confirmed by computer simulations (9, 10) where even in relatively small systems of 10^5 to 10^6 particles a box-sized aggregate is formed very soon, but the ultimate formation of one single aggregate requires a tenfold increase of the elapsed simulation time. On this basis the usual time necessary for formation of micron-sized aggregates as observed with STXM may be in the order of months and years. Only when the silica solution is confined very rapidly to a small space during a relatively rapid drying process will micron-sized aggregates be formed by the accelerated diffusion.

In some STXM experiments aggregates are formed apparently from square particles. See Fig. 9 for a typical specimen. In this case fast drying of the droplet also triggered crystallization of salt (KCl) on top of the silica fractal aggregate. This salt was present because the silica solution was prepared by acidification using HCl of water glass, a high-pH solution of silica in KOH. Most of the silica aggregates observed by STXM did not show the rectangular features of salt crystals,

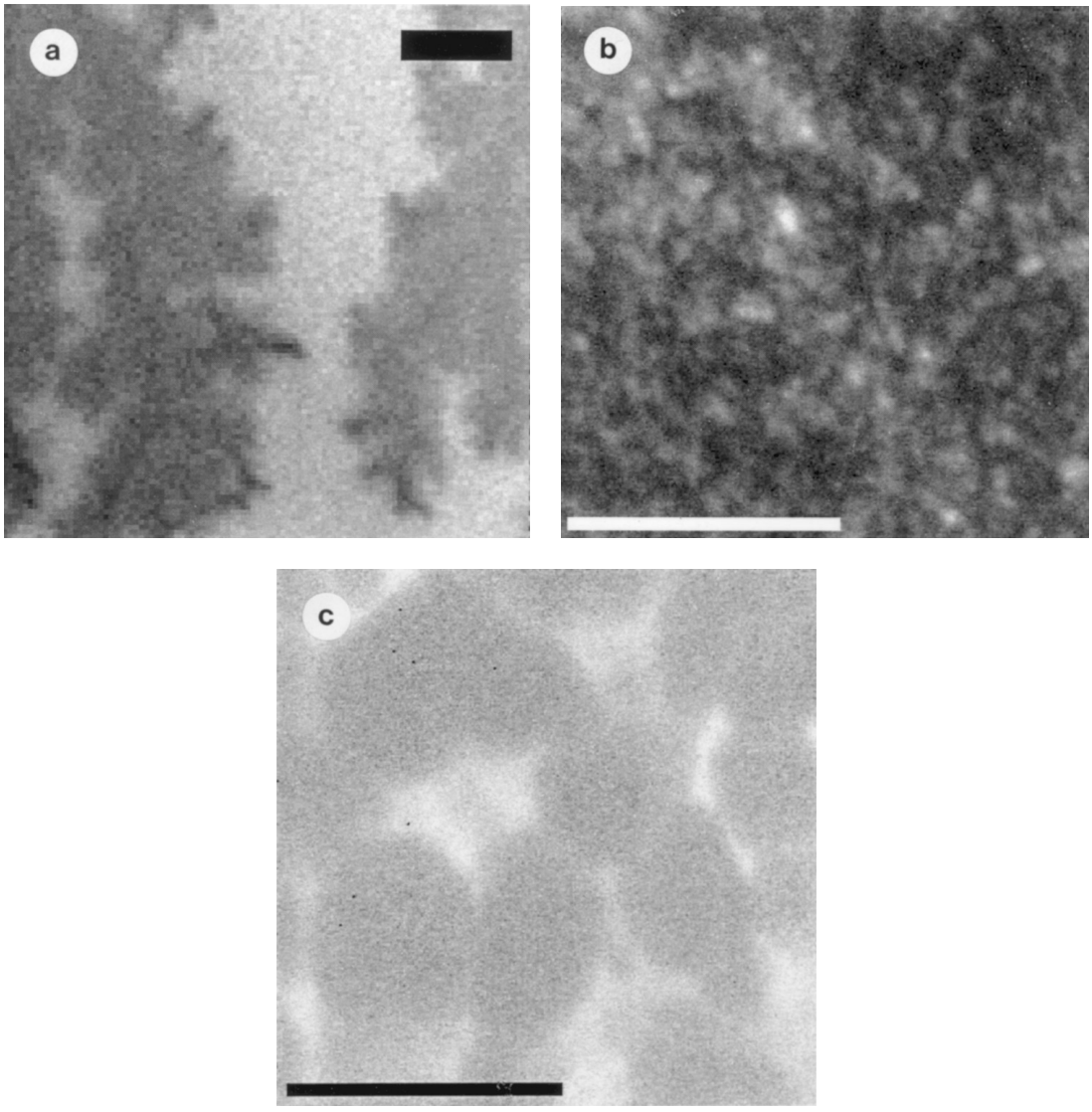

FIG. 12. Silicas prepared at pH 4 with no aging (a), aging during 48 h at 80°C (b) and aging during 24 days at room temperature (c). Bars are 7 μm (a), 5 μm (b), and 5 μm (c).

because in water glass KOH was replaced by NaOH which produces a more soluble salt, and the SiO_2/NaOH ratio was chosen as high as possible [3:1 (3)].

Because aggregates in solution could not be observed (due to thermal movements during image acquisition) and a gel could not be placed in a cell without destroying the vulnerable windows, cells were modified to permit slow and controlled evaporation of water. In this way we hoped to avoid the complete drying of the system and expected to immobilize the aggregates in the confined space, sufficiently to take sharp images. As mentioned in the experimental section, after addition of a small droplet silica solution in the cell, a second cell was placed on top of the first cell and both cells were partially glued together (see Fig. 5). Because only very narrow gaps were allowed, evaporation was extremely slow and as a result growth processes could be observed over a period of hours. A typical example is given in Fig. 10 where the formation of soluble silica structures at pH 7 is shown (with 0.4 wt % SiO_2 the solution is too diluted to form a gel) and the aging of silica can be studied ''in situ''.

With this method other aspects of the formation of silica can also be investigated. As shown in Fig. 6b and 11, the change of pH from 3 to 7 also affects the patterns at the micron scale. The images suggest that at pH 3 the particles (believed to be aggregates at the nanometer scale) are much smaller than at high pH, resulting in relatively fine-grained aggregates.

Very interesting aging effects are shown in Fig. 12. When no aging is applied, a micron-scaled fractal structure is present (Fig. 12a). After aging at 80°C no fractals could be

detected at the micron scale (Fig. 12b), but after aging instead at room temperature for 24 days relatively big lumps of silica are present (Fig. 12c).

CONCLUSIONS

With scanning transmission X-ray microscopy direct structural information can be obtained on micron-scale (0.05–100 micrometer). Using X-ray energies in the ''water window'' (380–480 eV) thin wet samples can be investigated if special cells controlling the evaporation of water are applied. As the examples above have shown, the STXM has now established itself as a viable tool for the study of hydrated silica systems. In a forthcoming paper we will present further results concerning the use of the X-ray microscope to study the aggregation, and gelation of silica, with particular regard to the influence of pH and aging conditions on the resulting structures.

ACKNOWLEDGMENTS

The authors gratefully acknowledge the financial support of the EPSRC (Grant GR/H63364 UK), NWO (The Netherlands) for granting beamtime at Daresbury, and The Netherlands Department of Economic Affairs (IOP-Katalyse; Program 89002-b) for financial support (H.F.v.G.). We also wish to thank P. A. F. Anastasi of King's College London for producing the silicon nitride membranes used to fabricate the specimen cells.

REFERENCES

1. Iler, R. K., ''The Chemistry of Silica.'' Wiley, New York, 1979.
2. Beelen, T. P. M., Wijnen, P. W. J. G., Rummens, C. P. J., and van Santen, R. A., ''Better Ceramics through Chemistry IV,'' MRS Symposium Proceedings, Vol. 180, p. 273. Materials Research Society, Pittsburgh, 1990.
3. Wijnen, P. W. J. G., Beelen, T. P. M., Rummens, C. P. J., Saeijs, H. C. P. L., de Haan, J. W., van de Ven, L. J. M., and van Santen, R. A., *J. Colloid Interface Sci.* **145,** 17 (1991).
4. Hench, L. L., and West, J. K., *Chem. Rev.* **90,** 33 (1990).
5. Brinker, C. J., and Scherer, G. W., ''Sol-Gel Science.'' Academic Press, San Diego, CA, 1990.
6. Mandelbrot, B. B., ''The Fractal Geometry of Nature.'' Freeman, New York, 1977.
7. Jullien, R., and Botet, R., ''Aggregation and Fractal Aggregates.'' World Scientific, Singapore, 1987.
8. Vicsek, T., ''Fractal Growth Phenomena,'' (2nd ed). World Scientific, Singapore, 1992.
9. van Garderen, H. F., Dokter, W. H., Beelen, T. P. M., van Santen, R. A., and Pantos, E., *Model. Simul. Mater. Sci. Eng.* **2,** 295 (1994).
10. van Garderen, H. F., Dokter, W. H., Beelen, T. P. M., van Santen, R. A., Pantos, E., Michels, M. A. J., and Hilbers, P. H. J., *J. Chem. Phys.* **102,** 480 (1995).
11. Beelen, T. P. M., van Garderen, H. F., Dokter, W. H., van Santen, R. A., and Pantos, E., ''Preparation of Catalysts VI,'' Symposium Proceedings, Studies in Surface Science and Catalysis, Vol. 91, p. 33. Elsevier, Amsterdam, 1995.
12. Knight, C. T. G., *J. Chem. Soc., Dalton Trans.* **1988,** 1457 (1988).
13. Wijnen, P. W. J. G., Beelen, T. P. M., de Haan, J. W., van de Ven, L. J. M., and van Santen, R. A., *Colloids Surf.* **45,** 255 (1990).
14. Ramsay, J. D. F., *Chem. Soc. Rev.* **15,** 335 (1986).
15. Dokter, W. H., Beelen, T. P. M., van Garderen, H. F., and van Santen, R. A., *in* ''Characterization of Porous Solids,'' Symposium Proceedings COPS III, Studies in Surface Science and Catalysis, Vol. 87, p. 725. Elsevier, Amsterdam, 1994.
16. Morrison, G. R., Bridgewater, S., Browne, M. T., Burge, R. E., Cave, R. C., Charalambous, P. S., Foster, G. F., Hare, A. R., Michette, A. G., Morris, D., and Taguchi, T., *Rev. Sci. Instrum.* **60,** 2464 (1989).
17. Morrison, G. R., and Burge, R. E., *in* ''Synchrotron Radiation X-Ray Spectroscopy'' (Hasnain, Ed.) p. 330. Ellis Horwood Limited, 1990.
18. Howells, M., Kirz, J., and Sayre, D., *Sci. Am.* **269,** 42 (1991).
19. Kirz, J., Jacobsen, C., and Howells, M., *Q. Rev. Biophys.* **28,** 33 (1995).
20. Sayre, D., and Chapman, H. N., *Acta Crystallogr.* **A51,** 237 (1995).
21. Beelen, T. P. M., Dokter, W. H., van Garderen, H. F., van Santen, R. A., Browne, M. T., and Morrison, G. R., ''Better Ceramics through Chemistry V,'' MRS Symposium Proceedings, Vol. 271, p. 263. Materials Research Society, Pittsburgh, 1992.
22. Shi, W. D., Morrison, G. R., Browne, M. T., Beelen, T. P. M., van Garderen, H. F., and Pantos, E., *Nucl. Instr. Methods Phys. Res. B* **97,** 202 (1995).
23. Morrison, G. R., Browne, M. T., Beelen, T. P. M., and van Garderen, H. F., *in* ''Soft X-Ray Microscopy'' (C. J. Jacobsen and J. E. Trebes, Eds.), Symposium Proceedings SPIE, Vol. 1741, p. 312. Society of Photo-Optical Instrumentation Engineers, Bellingham, Washington, 1992.
24. Morrison, G. R., Browne, M. T., Beelen, T. P. M., van Garderen, H. F., and Anastasi, P. H. F., *in* ''X-Ray Microscopy IV,'' Symposium Proceedings, p. 269. Moscow, 1994.
25. Thieme, J., Niemeyer, J., Guttmann, P., Wilhein, T., Rudolph, D., and Schmahl, G., *Progr. Colloid Polym. Sci.* **95,** 135 (1995).
26. Niemeyer, J., Thieme, J., Guttmann, P., Wilhein, T., Rudolph, D., and Schmahl, G., *Progr. Colloid Polym. Sci.* **95,** 139 (1995).
27. Tence, M., Chevalier, J. P., and Jullien, R., *J. Phys.* **47,** 1989 (1986).
28. Dokter, W. H., Beelen, T. P. M., van Garderen, H. F., van Santen, R. A., and Bras, W., *Angew. Chem.* **107,** 122 (1995).
29. Deutscher, G., and Lereah, Y., *Phys. Rev. Lett.* **60,** 1510 (1988).
30. Alexander, S., Bruinsma, R., Hilfer, R., Deutscher, G., and Lereah, Y., *Phys. Rev. Lett.* **60,** 1514 (1988).
31. Duan Jiang-zhong and Wu Zi-qin, *Solid State Commun.* **64,** 1 (1987).
32. Duan Jiang-zhong, Li Yan, and Wu Zi-qin, *Solid State Commun.* **65,** 7 (1988).
33. Allain, C., and Limat, L., *Phys. Rev. Lett.* **74,** 2981 (1995).
34. Honjo, H., and Ohta, S., *Phys. Rev. E* **49,** R1808 (1994).